



Research Article

## Experimental investigation of nanofluids for heat pipes used in solar photovoltaic panels

Bisma ALI<sup>1</sup>, Adnan QAYOUM<sup>2\*</sup>, Shahid SALEEM<sup>2</sup>, Fasil Qayoum MIR<sup>1</sup>

<sup>1</sup>Department of Mechanical Engineering, National Institute of Technology Srinagar, J&K, India

<sup>2</sup>Department of Chemical Engineering, National Institute of Technology Srinagar, J&K, India

### ARTICLE INFO

#### Article history

Received: 13 October 2021

Accepted: 16 February 2022

#### Keywords:

Nanoparticle; Nanofluid;  
Thermal Conductivity; Density;  
Therminol-55

### ABSTRACT

The current study is aimed to measure and analyze the impact of temperature ( $10^{\circ}\text{C} < T < 90^{\circ}\text{C}$ ) and particle concentration ( $0.05\% < \phi < 1.5\%$ ) on thermo-physical properties of  $\text{TiO}_2$ ,  $\text{ZnO}$  and  $\text{CuO}$  nanoparticles suspended in Therminol-55. The nanoparticles were characterized by using various techniques, including TEM, XRD, FTIR, TGA/DSC. TEM images reveal that the morphology of  $\text{TiO}_2$  and  $\text{ZnO}$  as spherical nanoparticles whereas that of  $\text{CuO}$  is in the form of flakes. XRD pattern for  $\text{TiO}_2$ ,  $\text{ZnO}$  and  $\text{CuO}$  nanoparticles possess anatase, hexagonal and monoclinic phase respectively. TGA results show that  $\text{TiO}_2$  losses less mass than the  $\text{ZnO}$  and  $\text{CuO}$  nanoparticles at each stage of decomposition. Thereby making it more stable thermally as compared to the other samples. Two-step method has been employed to formulate stable Therminol-55 based nanofluids containing  $\text{TiO}_2$ ,  $\text{ZnO}$  and  $\text{CuO}$  nanoparticles for varying particle concentrations. Results show that the thermal conductivity of suspensions containing solid conducting particles increase with increasing nanoparticle content and temperature of dispersions in the fluid. The thermal conductivity of  $\text{TiO}_2$ /Therminol-55,  $\text{ZnO}$ /Therminol-55 and  $\text{CuO}$ /Therminol-55 nanofluids increases up to 17.62%, 21.55% and 24.32% at particle concentration of 1.5 wt%. Further, the experimental results demonstrate that the density of nanofluids increased significantly with increase in concentration and decreased with temperature. Surface tension of nanofluids shows decrease with increase in particle concentration. This indicates that adding nanoparticles improve thermo-physical properties of nanofluid, making it suitable for use in heat pipe. The measured data for thermal conductivity and density are compared with existing theoretical models of nanofluids to check the effectivity of conventional models. A multi-variable new generalized correlations for thermal conductivity and density of Therminol-55 based nanofluids containing  $\text{TiO}_2$ ,  $\text{ZnO}$  and  $\text{CuO}$  nanoparticles are proposed.

**Cite this article as:** Bisma A, Adnan Q, Shahid S, Fasil Q M. Experimental investigation of nanofluids for heat pipes used in solar photovoltaic panels. J Ther Eng 2023;9(2):429–446.

\*Corresponding author.

\*E-mail address: [adnan@nitsri.ac.in](mailto:adnan@nitsri.ac.in)

This paper was recommended for publication in revised form by Regional Editor

Mustafa Kılıç



## INTRODUCTION

The world currently consumes around  $4.1 \times 10^{20}$  joules of energy per year, which is comparable to the continuous power consumption of 13 trillion watts (1). By 2050, global energy demand is expected to rise by 50%, and by the end of the century, it will be more than triple (2). Due to the detrimental impacts of fossil fuels, clean sustainable and alternative sources of energy are required to meet the demand. Solar energy is the primary source of clean and abundant energy for human progress and life on earth. Solar energy can be used to generate electricity either directly through solar photovoltaic (PV) modules or indirectly through thermal power plants. Solar photovoltaic technology is one of the renewable energy alternatives that has the potential to produce a cleaner, scalable, reliable and cost-effective electricity for the future. However, only around 15% of solar radiation is converted to electricity in a PV panel, with the rest converted to heat (1). When the working temperature of the PV module rises, the electrical efficiency decreases. As a result, decreasing the temperature of the PV module can improve its electrical efficiency. With the continuous progress in efficient energy systems, the need for design and fabrication of the efficient cooling system is indispensable (3,4).

Heat pipes are widely used as a novel cooling technique or as heat recovering systems. Heat pipes find numerous applications such as in solar energy, geothermal systems, space applications, telecommunications and electronic components etc (5–8). For these applications, light weight, small size and high performance are prerequisites for the current heat pipe design, especially for electronic systems (9). Heat pipe is an emerging passive heat transfer device that dissipates heat through phase-change mechanism. Heat pipe utilizes latent heat of vaporization of working fluid to transport heat from source to sink. Since heat pipes transfer heat through evaporation and condensation of working medium, the selection of working medium with improved thermo-physical properties is the key parameter for the efficient design and performance of heat pipe (4,5). The knowledge and understanding of thermal characteristic of working fluid are important for the design of heat pipes in various applications. Over the years, several techniques have been proposed to enhance the heat transfer characteristics. One of the recent attractive improvements in heat pipe working fluids is the use of nanofluids for achieving higher thermal efficiencies (10–12)

In recent years, metal and metal oxide nanoparticles have drawn vast attention due to their novel thermo-physical properties (13,14). With the requirement of further improvement in the performance of the present thermal systems, need for the next-generation fluids is expected. Nano technology has offered a new solution by introducing highly efficient heat transfer fluids with improved thermo-physical properties. These highly efficient heat transfer

fluids are known as Nanofluids, a term first proposed by Choi (15). Nanofluids are prepared by mixing nanometer-sized particles, with dimensions of less than 100 nm containing metals, carbides, oxides or carbon nanotubes in a conventional liquid such as water, acetone, oil and ethylene glycol (EG) etc. These colloidal suspensions of nano-sized particles can significantly improve the transport and thermal properties of the base fluid. Nano-fluid technology has advanced significantly in recent decades and proved its essential applications in cooling of electronic applications, petroleum industries, solar water heating, domestic refrigerator-freezers and in nuclear reactor etc. The main objective of using nanofluids is to exhibit high thermal conductivity at the most appropriate concentration ratio of nanoparticles. Nanofluids have been extensively used as heat transfer fluid (HTF) in engineering applications.

Numerous authors have performed experimental and numerical investigations to demonstrate the impact of varying temperature and particle loading range on improvement in thermal conductivity of various nanofluids. Muraleedharan et al. (16) reported the thermal conductivity study of  $\text{Al}_2\text{O}_3$ /Therminol-55 as the function of nanoparticle concentration (0.025-0.3 vol%). Results show that the thermal conductivity was enhanced by 11.7% for 0.1 vol%  $\text{Al}_2\text{O}_3$  concentration. Anish et al. (17) performed a series of experiments to characterize the thermal behaviour of  $\text{Al}_2\text{O}_3$ /Therminol-55 nanofluid at various particle concentrations (0.05-0.3%) and temperatures (30-50°C). Thermal conductivity of  $\text{Al}_2\text{O}_3$ /Therminol-55 nanofluid was found to have increased in accordance with an increment in the nanoparticle concentration and temperature. The best results for thermal conductivity enhancement was achieved at the particle concentration of 0.3% at 50°C.

The enhanced thermal conductivity of nanofluids offer several benefits, including higher cooling rates, lower pumping power requirements, smaller and lighter cooling systems, lower heat transfer fluid inventory, lower friction coefficients, and improved wear resistance. Those benefits make nanofluids promising for applications like coolants, lubricants, hydraulic fluids, and metal cutting fluids (18). Over the years, researchers have carried out various experiments in order to understand the underlying mechanisms responsible for the changes in physical properties of fluids with the addition of nanoparticles (19). Considering potential applications of nanofluids, not only thermal conductivity and viscosity are important, but surface tension and density should also be considered (20–23). In order to evaluate fluid dynamics and heat transfer performance of nanofluids, density and surface tension must be known.

Shoghl et al. (24) experimentally measured the densities of various water based nanofluids with copper oxide (CuO), Zinc oxide (ZnO), Aluminum oxide ( $\text{Al}_2\text{O}_3$ ), Carbon nanotube (CNT), Magnesium oxide (MgO) and Titanium oxide ( $\text{TiO}_2$ ) nanoparticles. Results show that the density increased with increase in nanoparticle concentration and

decreased with increase in temperature. Xie et al. (25) experimentally studied the density of Multi wall carbon nanotube (MWCNT) in an ionic-based fluid. It indicated that the nanofluid exhibits remarkable increase in density as compared to that of base fluid. Several investigations show that the presence of colloidal particles in a fluid causes the density to increase where as Vajjha et al. (21) and Jacquemin et al. (26) claim the opposite. The interfacial layer between nanoparticles and base fluid has been attributed for the discrepancies at higher volume fractions (27). The higher degree of aggregation reported at higher volume fractions was also responsible for large deviations (28). As a result, it is clear that predicting the effective density of nanofluids is difficult, and interfacial layer development and particle clustering are two crucial factors to consider.

While evaluating the performance of thermal systems, surface tension of heat transfer fluids is of high significance since this physical property influences the surface wettability and bubble growth (20). Wanic et al. (29) studied the surface tension of three different nitrides: titanium nitride, silicone nitride and aluminium nitride in Ethylene Glycol (EG) at a constant temperature of 298.15 K. Results show that the surface tension changes slightly with the addition of nanoparticles in the 1-5% mass concentration range. Harikrishan et al.(30) studied the surface tension of CuO-EG and Bismuth oxide  $Bi_2O_3$ -EG nanofluids. They observed that the surface tension decreased with mass concentration of nanoparticles in suspension.

Although reserachers have already worked in the field of nanofluids for some decades, comprehensive analysis of the thermo-physical properties of stable nanofluids is still required. Accurate measurment of physical properties are key to evaluate the potential applicability of these nanostructured heat transfer fluids in thermal systems. Furthermore there are no reports on effect of surface tension and density on Therminol-55 mixed with Titanium oxide , Zinc oxide and Copper oxide. This experimental work focuses on investigating the thermo-physical properties such as thermal conductivity, density and surface tension on nanofluids. The main purpose of this study is to

experimentally evaluate the effect of particle concentration ( $0.05\% < \phi < 1.5\%$ ) and temperature ( $10^\circ\text{C} < T < 90^\circ\text{C}$ ) on the thermal conductivity characteristics and density of Therminol-55 based  $TiO_2$ , ZnO and CuO mono nanofluids. Surface tension of nanofluids was evaluated for all the concentrations at the temperature of  $25^\circ\text{C}$ . The data obtained for thermal conductivity and density were compared with existing theoretical models and new correlations were developed for nanofluids.

## EXPERIMENTAL PROCEDURE

### Materials and Methods

Three different commercially available nanopowders  $TiO_2$ , ZnO and CuO (procured from Nanoshel, USA) were selected for this study. Lattice parameters were calculated from X-ray diffraction (XRD) data of crystal structure. These were suspended in Therminol-55 by two-step method. Therminol-55, used as base fluid, is a high temperature synthetic heat transfer fluid, which offers beneficial thermal features such as high boiling point and reasonably high viscosity at normal temperature (31–33). The various properties of nanoparticles and base fluid are given in Table 1 & 2.

For  $TiO_2$  nanoparticles lattice parameters were found to be  $a = b = 3.7830 \text{ \AA}$ ,  $c = 9.5024 \text{ \AA}$  and  $\alpha = \beta = \gamma = 90^\circ$ . For ZnO, lattice constants  $a = b = 3.24764 \text{ \AA}$  and  $c = 5.2027 \text{ \AA}$  and  $\alpha = \beta = 90^\circ$  and  $\gamma = 120^\circ$ . Similarly, for CuO, lattice parameters  $a = 4.6884 \text{ \AA}$ ,  $b = 3.4275 \text{ \AA}$  and  $c = 5.1234 \text{ \AA}$  and  $\alpha = \gamma = 90^\circ$  and  $\beta = 99.508^\circ$ .

The average crystallite size of  $TiO_2$ , ZnO and CuO nanoparticles can be estimated by using Debye Scherer equation.

$$D = K\lambda / \beta \cos\theta \tag{1}$$

where,  $D$  is the particle diameter size,  $K$  is 0.9 (Scherer's Constant),  $\lambda$  is the wavelength of the X-rays ( $\lambda=1.541858\text{\AA}$ ),  $\beta$  is the full width at half maximum (FWHM) of the diffraction peak and  $\theta$  is the Bragg diffraction angle.

**Table 1.** Thermophysical properties of nanoparticles

Physical Properties/ Parameters	TiO <sub>2</sub>	ZnO	CuO
Purity	>99%	>99%	>99%
Color	White	White	Black
Density (kg/m <sup>3</sup> )	4230	5600	6310
Specific surface area (m <sup>2</sup> /g)	10-45	35-45	21.5
Average particle size (nm)	10-25	10-30	<80
Molecular weight (g/mol)	79.866	81.38	79.54

**Table 2.** Physical, chemical and thermal properties of Therminol-55

Properties	Value
Appearance	Clear yellow liquid
Maximum bulk temperature	300°C (extended use up to 315°C)
Maximum film temperature	335°C
Kinematic viscosity @ 40°C	19mm <sup>2</sup> /s
Density @45°C	868 kg/m <sup>3</sup>

### Preparation of nanofluids

Three different nanofluids  $\text{TiO}_2/\text{Therminol-55}$ ,  $\text{ZnO}/\text{Therminol-55}$  and  $\text{CuO}/\text{Therminol-55}$  have been prepared for varying particle concentrations of 0.05%, 0.075%, 0.1%, 0.5%, 1% and 1.5 wt% using two-step method. In the two-step method, nanoparticles are produced separately and suspended in a base fluid. A sample of 50 ml has been prepared for each experiment. The amount of nanoparticles to be mixed in the base fluid for different particle concentrations is calculated by Equation 2 (34).

$$\% \varphi = \frac{\left[ \frac{W_{np}}{\rho_{np}} \right]}{\left[ \frac{W_{np}}{\rho_{np}} + \frac{W_{bf}}{\rho_{bf}} \right]} \quad (2)$$

where,  $\varphi$  is the particle concentration,  $w_{np}$  and  $w_{bf}$  represent the weight of nanoparticle and base fluid (grams),  $\rho_{np}$  and  $\rho_{bf}$  represent the density of nanoparticle and base fluid ( $\text{kg}/\text{m}^3$ ) respectively. Nanofluid stability is significantly important in order to produce a stable suspension to overcome agglomeration and sedimentation of particles. Oleic acid is used as dispersant with an aim of creating more stable nanofluids

as well as to maintain their thermo-physical properties for a long period of time. Oleic acid is used as dispersant, as it is highly miscible and has a viscosity comparable with Therminol-55 (35). Three different mono samples were fabricated with Oleic acid content of 0.5 ml per grams of nanoparticles (16,33).

In order to reach uniform distribution of nanometer-sized particles in the base fluid, each sample with the calculated quantity of nanoparticle concentration of 0.05, 0.075, 0.1, 0.5, 1 and 1.5% is added to the mixture of base fluid and the surfactant and then the mixture is stirred with a magnetic stirrer for 3 hours. Next the mixtures of  $\text{TiO}_2/\text{Therminol-55}$ ,  $\text{ZnO}/\text{Therminol-55}$  and  $\text{CuO}/\text{Therminol-55}$  have been sonicated at 20 kHz frequency for 4, 5 and 6 hours (32,36,37) respectively using a 120W ultrasonic device to break down the agglomeration between the nanoparticles. No sedimentation or precipitation is observed for a long time before the experiments. The resulting nanofluids exhibit uniform dispersion and are stable. The schematic of the experimental procedure used for preparation of nanofluids with varying concentration is shown in Figure 1.

### Instrumentation for characterization of nanoparticles

The morphological characterization of the nanoparticles was conducted by using Transmission Electron Microscope

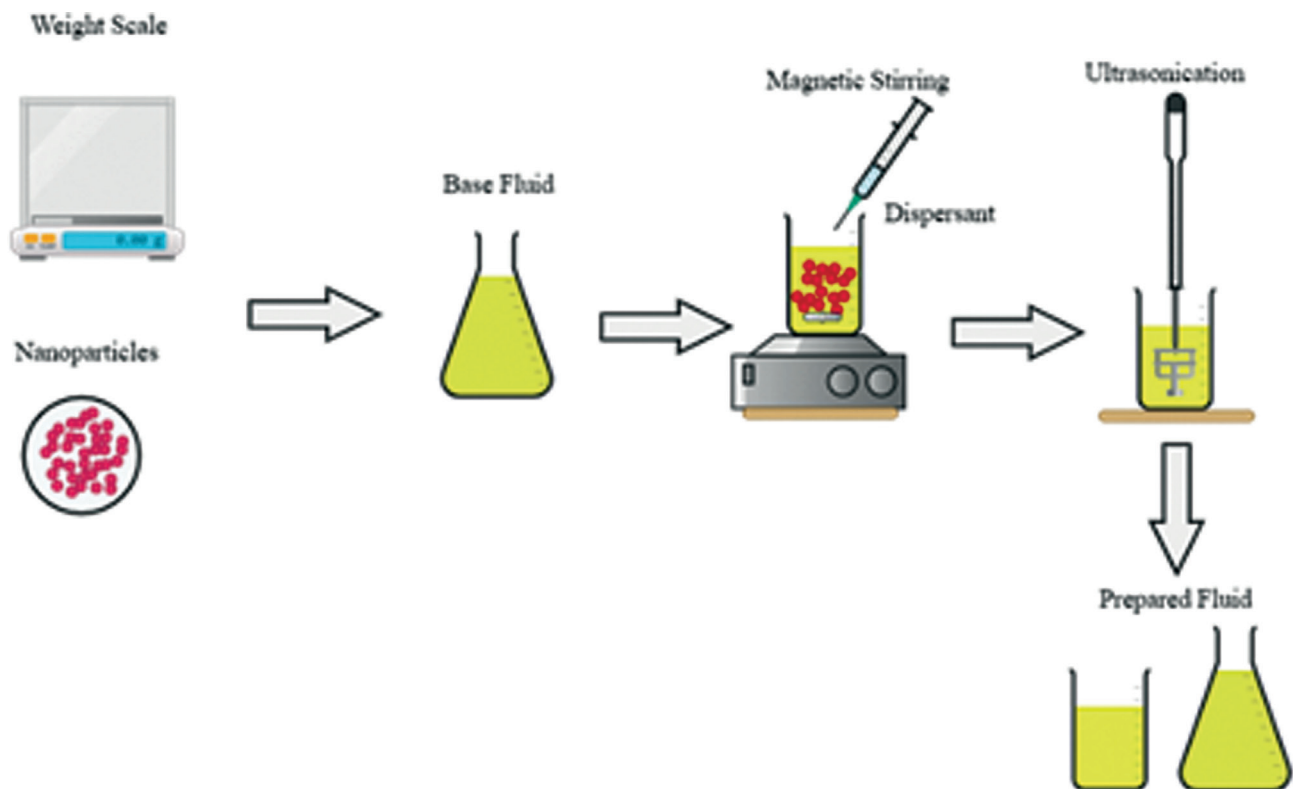


**Figure 1.** Schematic of the experimental procedure adopted for preparation of nanofluids.

(TEM) Jeol/JEM-1400 with a maximum accelerating voltage of 120 kV. The crystal structure and crystalline phases of nanoparticles were determined by X-ray diffraction (XRD) using a Rigaku diffractometer equipped with Cu K $\alpha$  radiation ( $\lambda=1.541858\text{\AA}$ ) within the range of 2 theta 5° to 90°. Fourier Transform Infra-Red (FTIR) spectral measurements were obtained to identify the presence of various functional groups within the compound. The FTIR spectra were collected and studied using (CARY 630, Agilent Technologies, USA) in the wavelength range of 600-4000  $\text{cm}^{-1}$ . Thermogravimetric Analysis (TGA) and Differential Scanning Calorimetry (DSC) is an effective tool to study the thermal behaviour of nanoparticles and its stability. TGA and DSC was conducted using Mettler Toledo TGA/DSC 3+/HT with alumina crucible.

#### Stability analysis of nanofluids using zeta potential

The stability of nanofluids is critical in order to maintain its thermo-physical properties for a long period of time. Nanofluids tend to agglomerate due to interactive forces, leading to formation of large clusters that settle rapidly and hence deteriorates the dispersion stability of nanofluids. To improve the stability of colloidal suspensions surfactants or dispersants are generally used. In the present study, Oleic acid is used as surfactant, which lowers the interactive forces between the particles themselves and between the particles and surrounding liquids (38). This phenomenon increases the immersion of particles and can prevent particle aggregation and ensure prolonged stability of nanofluids. The stability of suspensions was determined by measuring zeta potential for each sample by using AntonPaar Litesizer 500.

#### Measurement of thermo-physical properties

##### Thermal conductivity measurement

A KD2 Pro thermal property analyzer (Decagon Devices, Inc., USA), uses transient hot-wire method for thermal conductivity data measurement of nanofluids at a temperature ranging from 10°C-90°C with varying solid concentration of 0.05-1.5 wt%. The instrument mainly operates using a transient line heat source technique to measure the thermal conductivity of a liquid medium. The device consists of a handheld controller and a stainless steel 60 mm long KS-1sensor, with 1.3 mm diameter. For precise measurement, the sensor was vertically immersed into the sample to eliminate forced convection. To avoid experimental error, three set of measurements were conducted on each sample and their average values were recorded.

##### Density and surface tension

The density was measured by using a portable density meter (Anton Paar, DMA 4500M). The density of nanofluids was measured at the temperature varying from 10°C to 90°C and with varying concentration of 0.05wt% to 1.5wt%. This device can measure the density within the range of

0-3g/cm<sup>3</sup> with the precision of  $\pm 0.001\text{g/cm}^3$ . These density meters are based on the oscillating U-tube principle. The sample is injected with the help of a syringe through a filling nozzle into the measuring cell. A minimum of 1.5 ml of sample is required. All data was recorded for three times and an average value has been taken for the analysis.

## RESULTS & DISCUSSION

### Characterization of nanoparticles

#### Characterization of nanoparticles using TEM

Figures 2 show the typical transmission electron microscope images (Scale bar = 100 nm) of TiO<sub>2</sub>, ZnO and CuO nanoparticles respectively. As shown in the Figure, the

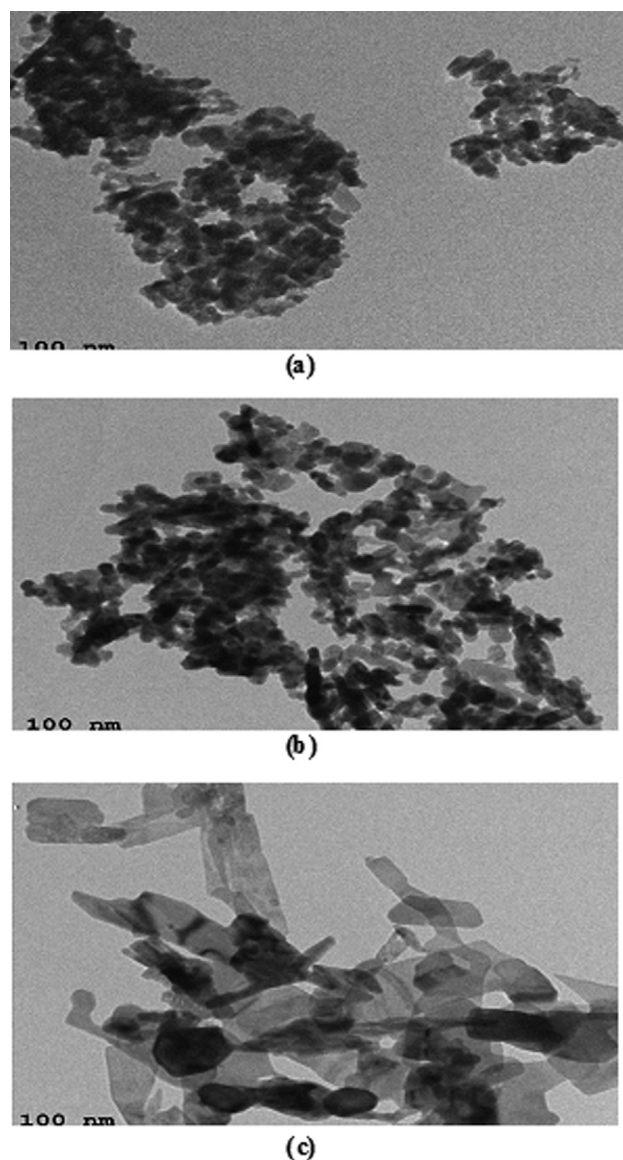


**Figure 2.** Typical TEM images of (a) TiO<sub>2</sub> (b) ZnO (c) CuO nanoparticles.

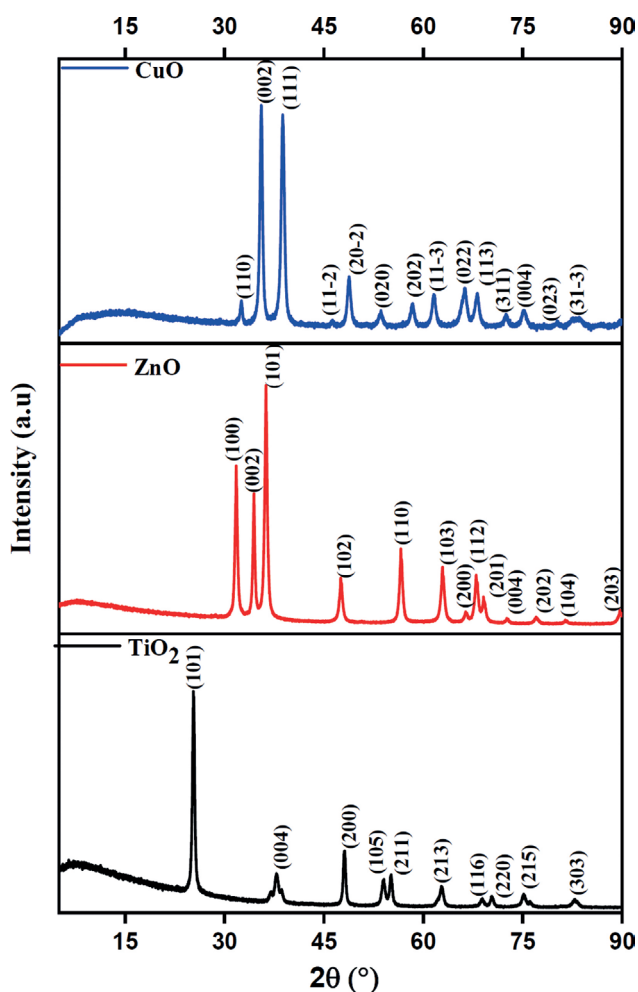


Figure 3. X-ray diffraction patterns of three different nanoparticles.

morphology of  $\text{TiO}_2$  and  $\text{ZnO}$  nanoparticles is approximately spherical whereas that of  $\text{CuO}$  is in the form of flakes.

#### Characterization of nanoparticles using X-ray diffraction (XRD)

Figure 3 shows the X-ray diffraction (XRD) patterns for  $\text{TiO}_2$ ,  $\text{ZnO}$  and  $\text{CuO}$  nanoparticles. XRD pattern of  $\text{TiO}_2$  nanoparticles indicate anatase structure as indicated by the strong peaks with reflection planes at  $25.32^\circ$  (101),  $37.83^\circ$  (004),  $48.08^\circ$  (200),  $53.97^\circ$  (105),  $55.11^\circ$  (211),  $62.86^\circ$  (213),  $68.87^\circ$  (116),  $70.36^\circ$  (220),  $75.18^\circ$  (215) and  $82.88^\circ$  (303). The prominent peaks are in good agreement with the reference patterns reported by the JCPDS Card No.00-064-0863.

$\text{ZnO}$  exhibit hexagonal wurtzite structure as indicated by the broad peaks having 2 theta values with reflection planes at  $31.75^\circ$  (100),  $34.47^\circ$  (002),  $36.25^\circ$  (101),  $47.56^\circ$  (102),  $56.63^\circ$  (110),  $62.9^\circ$  (103),  $66.45^\circ$  (200),  $68.01^\circ$  (112),

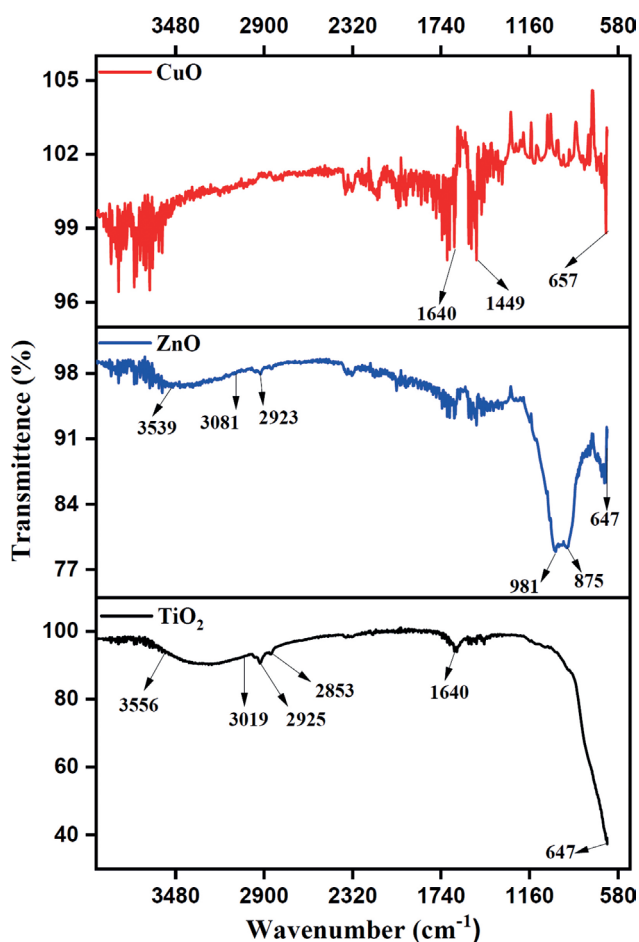


Figure 4. FTIR spectrum of  $\text{TiO}_2$ ,  $\text{ZnO}$  and  $\text{CuO}$  nanoparticles.

$69.13^\circ$  (201),  $72.65^\circ$  (004),  $77.05^\circ$  (202),  $81.26^\circ$  (104) and  $89.74^\circ$  (203) corresponds to JCPDS Card No.01-080-3030.

$\text{CuO}$  nanoparticles possess monoclinic phase. The peaks at  $32.52^\circ$  (110),  $35.53^\circ$  (002),  $38.77^\circ$  (111),  $46.29^\circ$  (11-2),  $48.77^\circ$  (20-2),  $53.55^\circ$  (020),  $58.34^\circ$  (202),  $61.58^\circ$  (11-3),  $66.27^\circ$  (022),  $68.14^\circ$  (113),  $72.52^\circ$  (311),  $75.20^\circ$  (004),  $80.26^\circ$  (023) and  $83.1^\circ$  (31-3) correspond to  $\text{CuO}$  diffraction peak. The obtained peaks are in good accord with those in the JCPDS card (Card No.01-080-1917).

The average crystallite size of the  $\text{TiO}_2$ ,  $\text{ZnO}$  and  $\text{CuO}$  nanoparticles calculated using Debye Scherer formula was about 16.9 nm, 18.7nm and 16.12nm respectively.

#### Characterization of nanoparticles using Fourier transform infra-red spectroscopy (FTIR)

Figure 4 shows the FTIR spectra of  $\text{TiO}_2$ ,  $\text{ZnO}$  and  $\text{CuO}$  nanoparticles. Metal oxides generally give absorption bands in fingerprint regions below  $1000\text{cm}^{-1}$  emerging

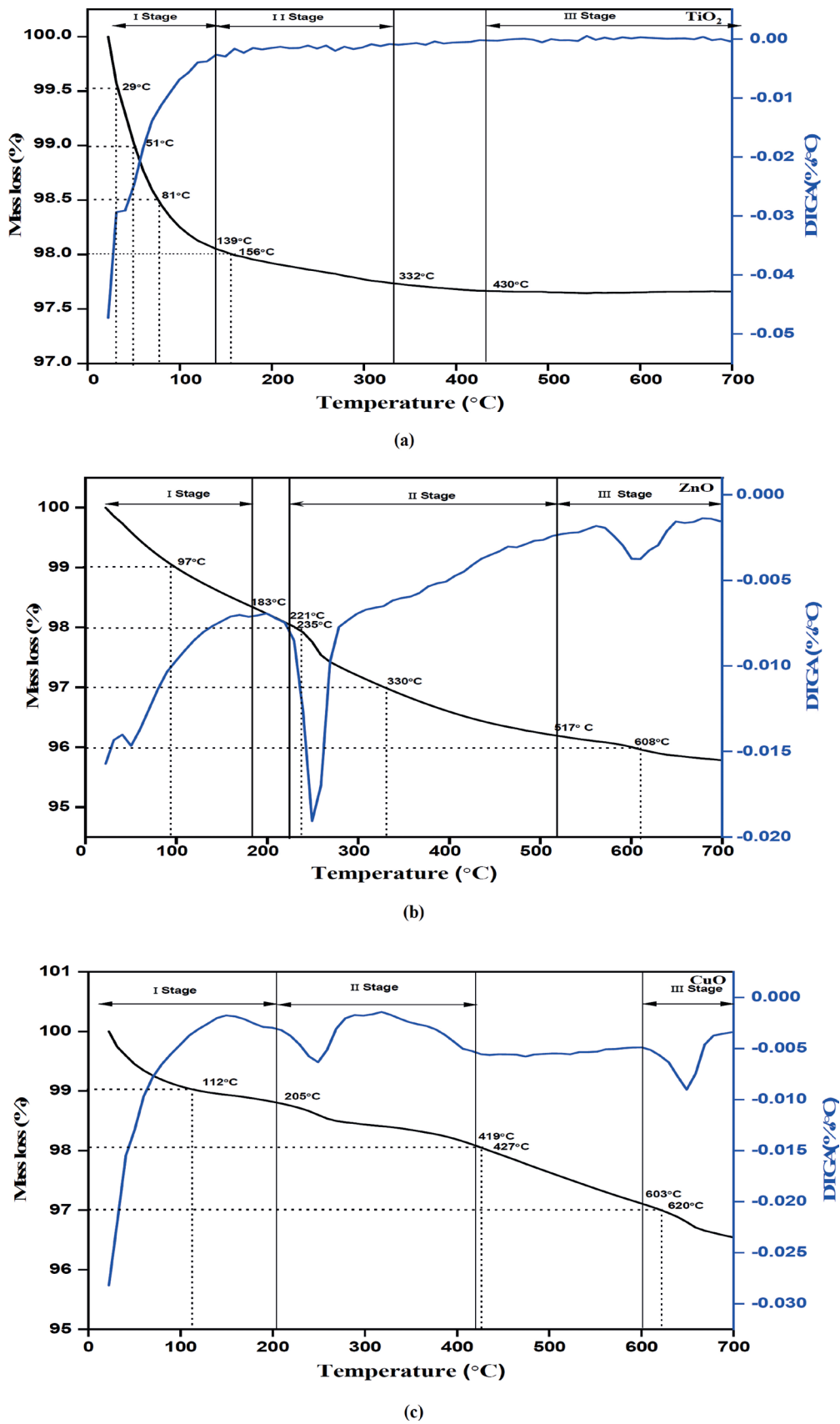
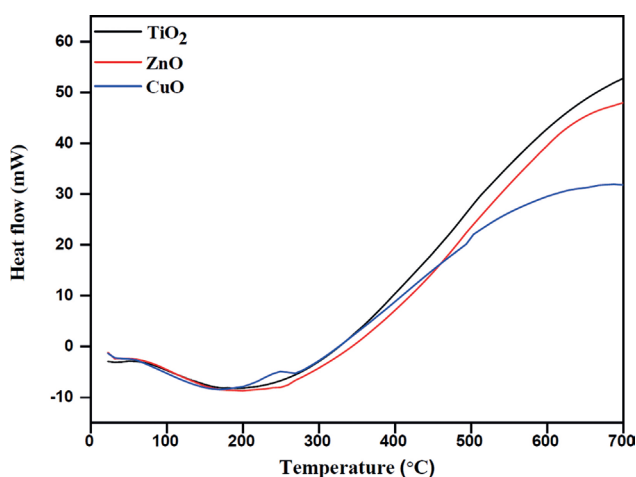


Figure 5. TGA-DTGA curves of (a) TiO<sub>2</sub> (b) ZnO (c) CuO nanoparticles.

**Table 3.** Mass loss (%) at different stages of degradation

Sample	First stage of degradation Temperature (°C)	Mass loss (%)	Second stage of degradation Temperature (°C)	Mass loss (%)	Third stage of degradation Temperature (°C)	Mass loss (%)
TiO <sub>2</sub>	23-139	1.91	139-332	0.324	430-700	0.006
ZnO	22-283	1.61	221-517	1.858	517-700	0.438
CuO	23-205	1.17	205-419	0.698	603-700	0.586

**Figure 6.** Differential scanning calorimetry curves of three different nanoparticles.

from interatomic vibration (39). For TiO<sub>2</sub> nanoparticle, the absorbance bands observed between 3500-3000 cm<sup>-1</sup> are attributed to hydroxyl (O-H) stretching (40). Peaks at 2923 cm<sup>-1</sup> and 2853 cm<sup>-1</sup> corresponds to the C-H stretching vibrations (41). Peak at 1640 cm<sup>-1</sup> corresponds to C=O vibrations (39–41).

For ZnO nanoparticle, the peaks arising between 3539-3081 cm<sup>-1</sup> and 981-875 cm<sup>-1</sup> are assigned to O-H and C-N stretching (40,42). Peaks at 2923 are due to sp<sup>3</sup> C-H stretching vibrations (43). Peaks present in the region 656-500 are the characteristic absorption peaks of ZnO stretching vibration frequency (44).

In the FTIR spectrum of CuO nanoparticles, the peak at 1640 indicates C=C stretching and 1449 indicates aromatic ring stretching (45). Peaks present in the region 660-600 indicate stretching vibrations of Cu-O bond (46).

#### Characterization of nanoparticles using thermogravimetric analysis (TGA) and DTGA

The thermal behavior and stability of TiO<sub>2</sub>, ZnO and CuO nanoparticles was analyzed by using TGA and DSC techniques over the temperature range of 30-700°C under

a uniform heating rate of 10°C min<sup>-1</sup>. (TGA) and (DTGA) of the three different nanoparticles are shown in Figure 5. The TGA curves in the above Figures clearly indicate that the weight loss of the given nanoparticles is the function of temperature. DTGA curves are calculated as the temperature derivative of the remaining mass percentage from the TGA analysis. TGA curves display three main stages of mass loss. Table 3 and Figure 5 shows that the first stage of decomposition of the nanoparticles start from a temperature range of 23-139°C for TiO<sub>2</sub>, 22-183°C for ZnO nanoparticles and 23-205°C for CuO. The mass loss of the samples for the TiO<sub>2</sub> nanoparticles is up to 1.91%, 1.61% for ZnO and 1.17% for CuO nanoparticles. The mass loss in first stage originates mainly due to release of absorbed water (47).

The second stage of degradation occurs in the temperature range of 139-332°C for TiO<sub>2</sub>, 221-517°C for ZnO and 205-419°C for CuO nanoparticles which is attributed to the evaporation and dehydration of absorbed free and coordinated water molecules from the nanoparticle samples. The second stage shows the mass loss of 0.32% for TiO<sub>2</sub>, 1.85% for ZnO and 0.69% for CuO nanoparticles respectively.

The third stage of degradation shows negligible mass loss. From the curves it is evident that at higher temperatures, no further significant mass loss was observed. There is less percentage drop in mass loss i.e. 0.006% for TiO<sub>2</sub>, 0.438% for ZnO and 0.586% for CuO nanoparticles. It has been observed from the above TGA and DTGA curves that TiO<sub>2</sub> losses less mass than the ZnO and CuO nanoparticles at each stage of decomposition. Hence it is more thermally stable as compared to the other two samples. The major DTGA peaks reach the temperature about 43°C for TiO<sub>2</sub>, 249°C, 603°C for ZnO and 247°C, 648°C for CuO nanoparticles.

#### Characterization of nanoparticles using differential scanning calorimetry (DSC)

DSC is a thermal analytical technique that measures the heat flow in and out associated with sample as a function of temperature. The DSC curve for three different samples is shown in Figure 6. The endothermic process starts from 130°C to 270°C. The DSC curve of TiO<sub>2</sub>, ZnO and CuO

show the presence of a common wide endothermic peaks 219°C, 230°C and 193°C respectively.

### Nanofluids stability

Zeta potential analysis is an efficient approach to characterize the stability of suspensions quantitatively. Two tests were performed on each sample immediately after 2 hour and on 08th day of the sample preparation. Figure 7 indicates variation in zeta potential for varying particle concentrations of TiO<sub>2</sub>, ZnO and CuO in Therminol-55 on the 08<sup>th</sup> day of sample preparation. It is observed that the dispersion stability is maximum for nanoparticle concentration of 0.05 wt% for all three different nanofluids. The stability was observed to decrease with increase in particle concentration. In terms of stability, zeta potential of > ±30 mV are regarded to be stable (38,48,49). For TiO<sub>2</sub>/Therminol-55, ZnO Therminol-55 and CuO/Therminol-55 nanofluids the measured zeta potential varies from 56.7 to 43.1 mV, 53.2 to 37.5 mV and 49.2 to 30.1 mV with varying particle concentration of 0.05 wt% to 1.5 wt% respectively. Almost all the samples exhibit zeta potential above stability criterion. Visual inspection of all the samples which was done on 8<sup>th</sup>

day of preparation also confirm the stability as shown in Figure 8.

## THERMAL CONDUCTIVITY MEASUREMENTS

### Effect of particle concentration and temperature

In this section, the thermal conductivity characteristics of TiO<sub>2</sub>/Therminol-55, ZnO/Therminol-55 and CuO/Therminol-55 nanofluids were measured. Assorted parameters that affect the thermal conductivity of nanofluids such as: solid particle concentration, temperature, and thermal conductivity of base fluid as well as that of nanoparticles were analyzed. Thermal conductivity of nanofluids, as a function of temperature (10°C < T < 90°C) and nanoparticle loadings (0.05 < φ < 1.5 wt%), were investigated. Most of the experimental studies related to nanofluids focus on determining the role of varying temperature and solid particle concentration on overall enhancement of thermal conductivity (50). The general trend of the experimental results shows that the improvement in thermal conductivity significantly depends on nanoparticle loading and temperature. Further the experimental data obtained have been compared with the existing models to recognize the possible mechanisms responsible for the improvement in thermal conductivity, with increasing particle loading, at higher temperatures.

In order to provide a better physical insight, thermal conductivity of pure Therminol-55 was measured over the temperature range of 10°C to 90°C and compared with the literature values. Figure 9 represents variation of thermal conductivity for pure Therminol-55 with temperature. It is apparent from Figure 9 that the thermal conductivity for Therminol-55 decreases with temperature, mainly due to its high viscosity characteristic (35,37). The measured data for temperature dependence of pure Therminol-55 is in good agreement with the data provided by the manufacturers.

The effect of TiO<sub>2</sub>, ZnO and CuO nanoparticle concentration from (0.05 wt% to 1.5 wt %) on thermal conductivity ( $k_{nf}$ ) of TiO<sub>2</sub>/Therminol-55, ZnO/Therminol-55 and

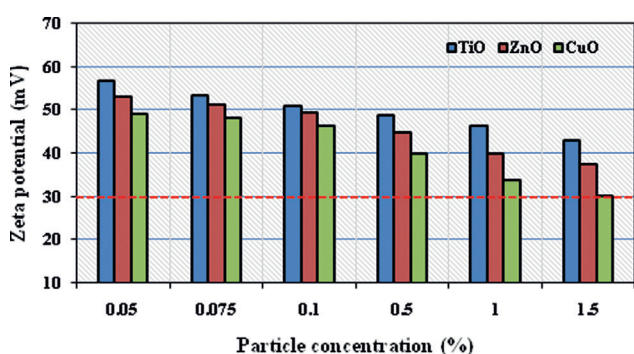


Figure 7. Zeta potential of TiO<sub>2</sub>, ZnO and CuO in Therminol-55 for varying concentration.

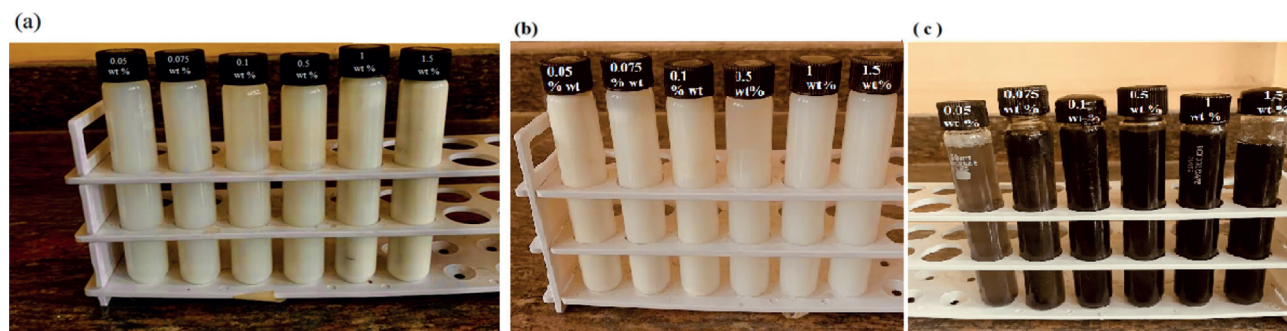


Figure 8. Visual inspection of a) TiO<sub>2</sub>/Therminol-55, b) ZnO/Therminol-55 and c) CuO/Therminol-55 nanofluids on 8<sup>th</sup> day of sample preparation.

CuO/Therminol-55 nanofluids at 27°C is shown in Figure 10. It is evident from the Figure 10 that the thermal conductivity of TiO<sub>2</sub>/Therminol-55, ZnO/Therminol-55 and CuO/Therminol-55 nanofluids increases with nanoparticle concentration. The thermal conductivity enhancement for TiO<sub>2</sub>, ZnO and CuO suspended in Therminol-55 nanofluids at 27°C shows maximum enhancement of 4.10, 5.11 and 5.68% at particle concentration of 1.5%.

Improvement in thermal conductivity is observed with addition of nanoparticles in base fluid, is ascertained to the higher intrinsic heat transfer capacity of TiO<sub>2</sub>, ZnO and CuO nanoparticles (37,51). At lower particle concentrations, the enhancement in thermal conductivity is less significant due to thermal contact resistance. Thermal conductivity is more distinguished at higher concentrations due to the formation of large particle clusters which further enhances the interactions between the nanoparticles, thereby transporting heat more efficiently (52). At higher concentration, due to the increase in the number of nanometer-sized particles in the base fluid, mean free path of nanoparticles gets reduced, resulting in higher intermolecular collisions and thus enhances the thermal conductivity of nanofluids (53,54). Higher thermal conductivity is obtained from all the samples with increasing particle concentration mainly due to the increase in number of nanoparticles available which results in more particle collisions between them. It should be noted that the excessive increase of solid particle concentration should be avoided to prevent precipitation, sedimentation and formation of particle chains which is not desirable. This is very well supported by the fact that in the experimental investigation particle loading should be limited to below 10 wt% (55).

Figure 11a show the variation of thermal conductivity of TiO<sub>2</sub>/Therminol-55 nanofluid with respect to temperature. Examining the experimental data from Figure 11a, for

0.05 wt% thermal conductivity increases from 0.1297 W/mK at 11.2°C to 0.1330 W/mK at 89.8°C. Similarly, for particle loading of 1.5 wt%, thermal conductivity changes from 0.1346 W/mK at 9.8°C to 0.1415 W/mK at 89.7°C.

Figure 11b represents thermal conductivity of ZnO/Therminol-55 nanofluid as a function of temperature. For 0.05 wt% ZnO/Therminol-55 nanofluid, thermal conductivity increases from 0.1309 W/mK at 11.7°C to 0.1373 W/mK at 88.4°C. Similarly, for 1.5 wt% thermal conductivity changes from 0.1367 W/mK at 11.2 °C to 0.1460 W/mK at 88.2°C.

Thermal conductivity of CuO/Therminol-55 nanofluid with respect to temperature is shown in figure 11c. For CuO/Therminol-55 nanofluid with particle concentration of 0.05 wt% thermal conductivity attains value of 0.1324 W/mK at 9.6°C to 0.1388 W/mK at 88.5°C. Similarly, for particle concentration of 1.5 wt%, thermal conductivity increases from 0.1392 W/mK at 10.8°C to 0.1501 W/mK at 88.5°C showing the significant contribution of augmented temperature and particle concentration on thermal conductivity. An almost similar increasing trend of thermal conductivity of nanofluid has been observed for the various volume concentration and temperature by Gulzar et al. (31), Anish et al. (17) and Muraleedharan et.al. (16).

The highest value for thermal conductivity for each of the nanofluids was observed to be at the condition where temperature and concentration is at the maximum. It is evident that as the temperature increases, thermal conductivity undergoes an increase that is more distinguished. The main reason can be attributed to the higher intensity of nanoparticles which increase the Brownian motion and larger interactions between the nanoparticles, which in turn enhances the thermal conductivity meaningfully (56–58). Though Brownian motion plays a critical role for

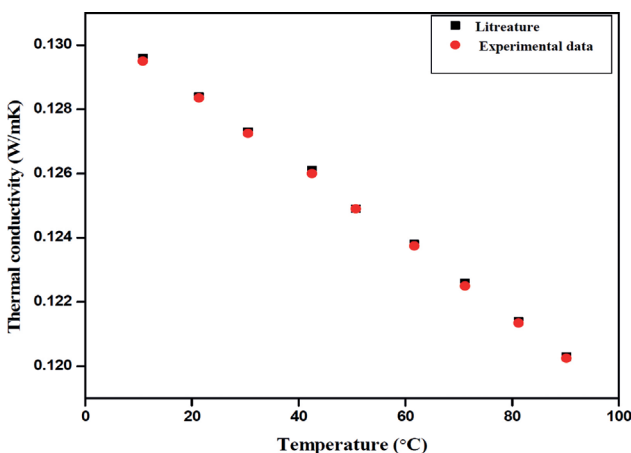


**Figure 9.** Influence of temperature on thermal conductivity of pure Therminol-55.

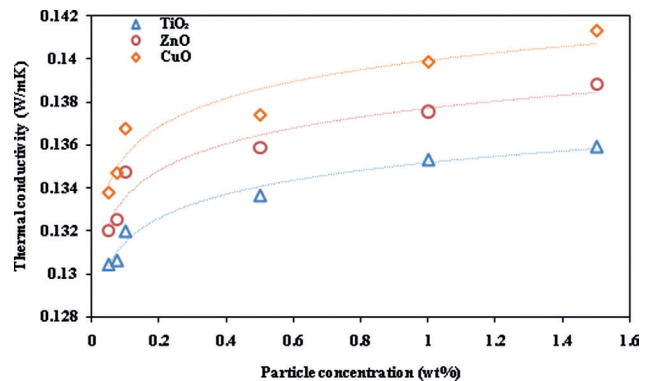


**Figure 10.** Effect of nanoparticle concentration on thermal conductivity of TiO<sub>2</sub>/Therminol-55, ZnO/Therminol-55 and CuO/Therminol-55 nanofluids at 27°C.

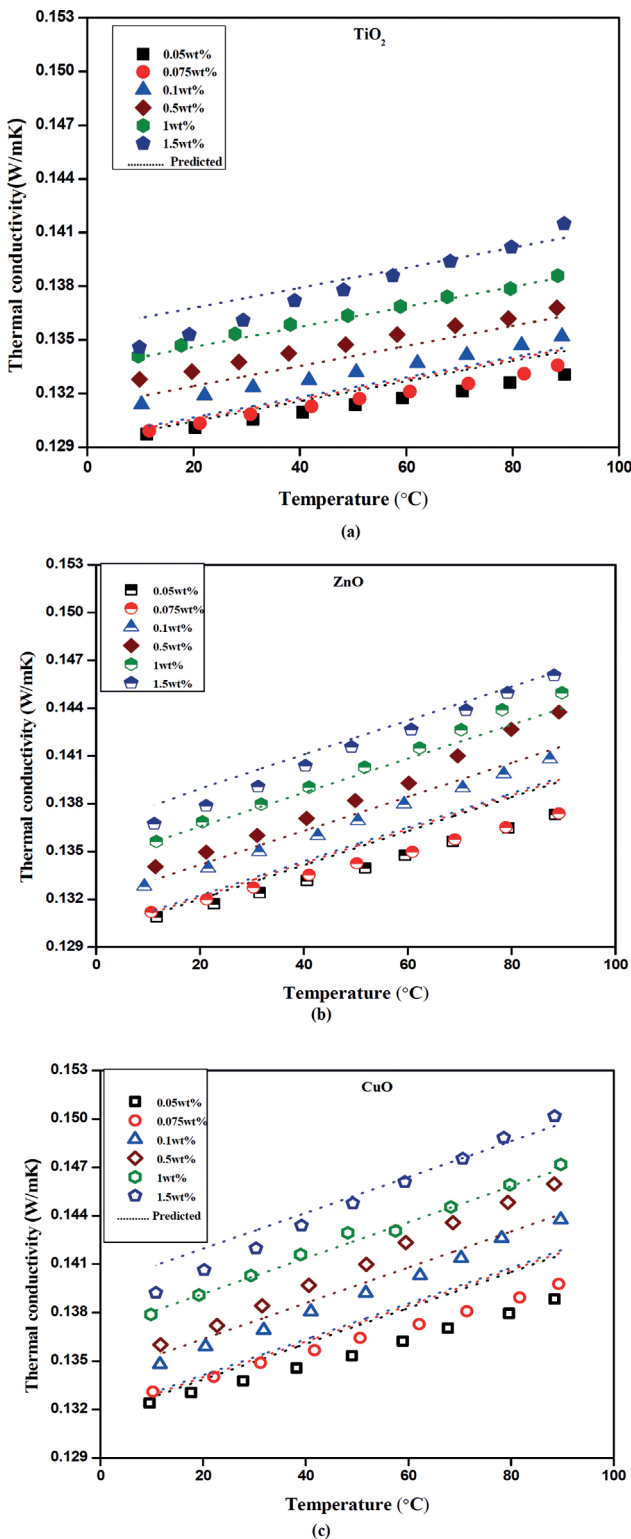


**Figure 11.** Influence of temperature on thermal conductivity of (a) TiO<sub>2</sub>/Therminol-55 (b) ZnO/Therminol-55 and (c) CuO/Therminol-55 nanofluids with varying particle concentration.

the thermal conductivity enhancement with temperature, associated with nanoscale mechanisms, the effects of particle clustering, higher aspect ratio of the particle and liquid layering also contribute to increased thermal conductivity significantly (54,59). At higher particle concentration and temperature, both Brownian motion and particle clustering work together to enhance the thermal conductivity more distinctly.

The thermal conductivity enhancement for TiO<sub>2</sub>, ZnO and CuO suspended in Therminol-55 nanofluids shows maximum enhancement of 17.62, 21.55 and 24.32% at particle concentration of 1.5%. The enhancements in thermal conductivity of each nanofluid of particle concentration (0.05-1.5%) are not uniform with increase in temperature. At higher temperature, the interfacial thermal resistance increases with increasing temperature, which leads to decrease in thermal conductivity enhancement in nanofluids. Xie et al. (61) and Said et al. (62) observed that the increment in thermal conductivity of nanofluids are proportional with respect to nanoparticle volume concentration. However, Moosavi et al. (56) and Nadoosan (58) found that the thermal conductivity enhancement has a nonlinear relation with respect to volume fraction.

Several theories to explain the possible anomalous enhancement in thermal conductivity with an emphasis to provide additional physical insight on possible mechanism to evaluate the enhanced thermal conductivity of nanofluids have come to light. Accordingly, the experimental data obtained is compared with the existing classical models for solid-liquid mixtures (56). Maxwell model and Hamilton-Crosser model have been used for comparison of the thermal conductivity ratio obtained from these experimental measurements.

Maxwell’s model (63) is written as:

$$\frac{k_{nf}}{k_{bf}} = \frac{k_{np} + 2k_{bf} + 2(k_{np} - k_{bf})}{k_{np} + 2k_{bf} - (k_{np} - k_{bf})} \quad (3)$$

Hamilton Crosser model (64) is written as:

$$\frac{k_{nf}}{k_{bf}} = \frac{k_{np} + (n-1)k_{bf} - (n-1)(k_{bf} - k_{np})}{k_{np} + (n-1)k_{bf} + (k_{bf} - k_{np})} \quad (4)$$

where  $k_{np}$  and  $k_{bf}$  refers to the thermal conductivity of added nanosized particles and Therminol-55,  $\phi$  is the particle volume fraction of the solid particles (vol%),  $n$  is the empirical shape factor given by  $n = 3/\Psi$  and  $\Psi$  is the particle sphericity and is defined as ratio of the surface area of a sphere (with volume equal to that of the particle) to the surface area of the particle. For a spherical shaped particle,  $\Psi = 1$  and  $n = 6$  is the empirical shape factor considered for flakes (65). Comparison of thermal conductivity with Maxwell and Hamilton Crosser model using Equation 3 and 4 for three different nanofluids are represented in

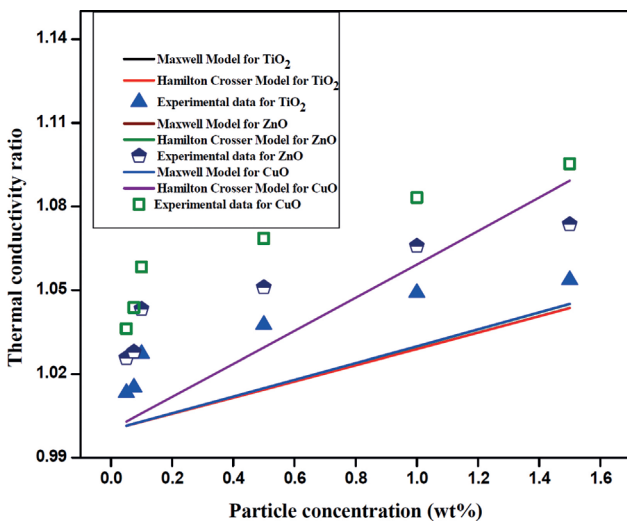


**Figure 12.** Comparison of thermal conductivity ratio of (a)  $\text{TiO}_2$  (b)  $\text{ZnO}$  (c)  $\text{CuO}$ / Therminol-55 nanofluids with Maxwell's and Hamilton Crosser theoretical model.

Figure 12. Since  $\Psi = 1$ , for spherical shaped particles the result obtained from both the above-mentioned theoretical models will be same. The data obtained from the above-mentioned models do not match with our experimental results. The existing classical models distinctly overestimate the experimental results, hence cannot precisely predict the trends observed in determining the thermal conductivity of nanofluids. Maxwell equation is a good choice for spherical shaped, low particle concentration and for liquids containing micro particles. Hamilton Crosser model is the modified version of Maxwell model and incorporates the effect of particle shape, used for predicting the thermal conductivity of both spherical as well as solid-liquid mixtures containing non-spherical shaped particles.

Because of lack of suitable and reliable correlation to estimate thermal conductivity of nanofluids, new correlations have been developed from the experimental data as a function of temperature and particle concentration. These correlations are valid in the temperature range of  $10^\circ\text{C}$  to  $90^\circ\text{C}$  and particle concentration range of  $0.05\text{wt}\%$  to  $1.5\text{wt}\%$ . Equations 5, 6 and 7 proposes a multivariable correlation obtained from multiple linear regression model for the thermal conductivity of  $\text{TiO}_2$ /Therminol-55,  $\text{ZnO}$ /Therminol-55 and  $\text{CuO}$ /Therminol-55 nanofluids. The co-efficient of regression ( $R^2$ ) has been found to be 92.14%, 90.88% and 91.01% for  $\text{TiO}_2$ /Therminol-55,  $\text{ZnO}$ /Therminol-55 and  $\text{CuO}$ /Therminol-55 nanofluids respectively.

For  $\text{TiO}_2$ /Therminol-55,

$$k_{\text{nf}} = 0.129113 + 0.0000561264T + 0.00437474\phi \quad (5)$$

$$R^2 = 92.14\%$$

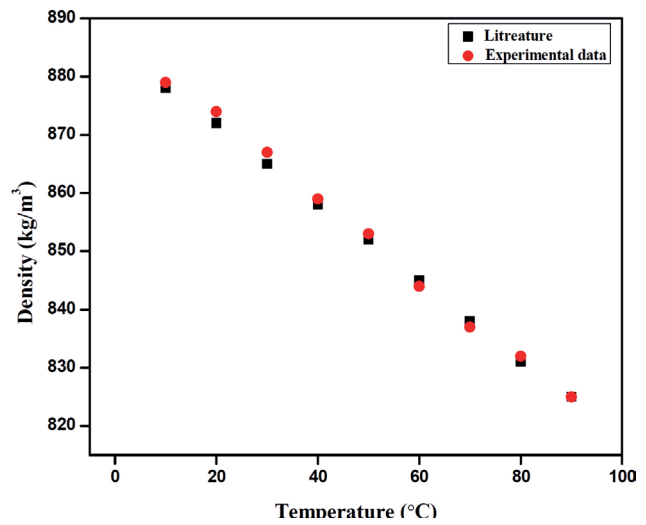


**Figure 13.** Impact of temperature on density of Therminol-55.

For  $\text{ZnO}$ /Therminol-55,

$$k_{\text{nf}} = 0.129640 + 0.000106674T + 0.00478609\phi \quad (6)$$

$$R^2 = 90.88\%$$

For  $\text{CuO}$ /Therminol-55,

$$k_{\text{nf}} = 0.1313353 + 0.000110933T + 0.00559339\phi \quad (7)$$

$$R^2 = 91.01\%$$

The experimental data for thermal conductivity of  $\text{TiO}_2$ /Therminol-55,  $\text{ZnO}$ /Therminol-55 and  $\text{CuO}$ /Therminol-55 nanofluids were shown in Figures 11 a, b and c respectively, along with the predicted values from equations 5 to 7.

## MEASUREMENT OF DENSITY OF NANOFLUIDS

### Effect of particle concentration and temperature on density

For a more detailed evaluation of effectiveness of nanofluids, influence of particle concentration and temperature on thermo-physical properties is the most crucial and key parameter for the fluid flow characteristic and system design. For this purpose, the variation of nanofluid density with concentration and temperature has been investigated. The density of base fluid was measured at temperatures varying from  $10^\circ\text{C}$  to  $90^\circ\text{C}$  and the results were compared with the data in literature presented in Figure 13. An excellent agreement is observed between the current measurements and the data available in literature.

The density of Therminol-55 based  $\text{TiO}_2$  nanofluid at different temperature ( $10^\circ\text{C}$ - $90^\circ\text{C}$ ) and particle concentration

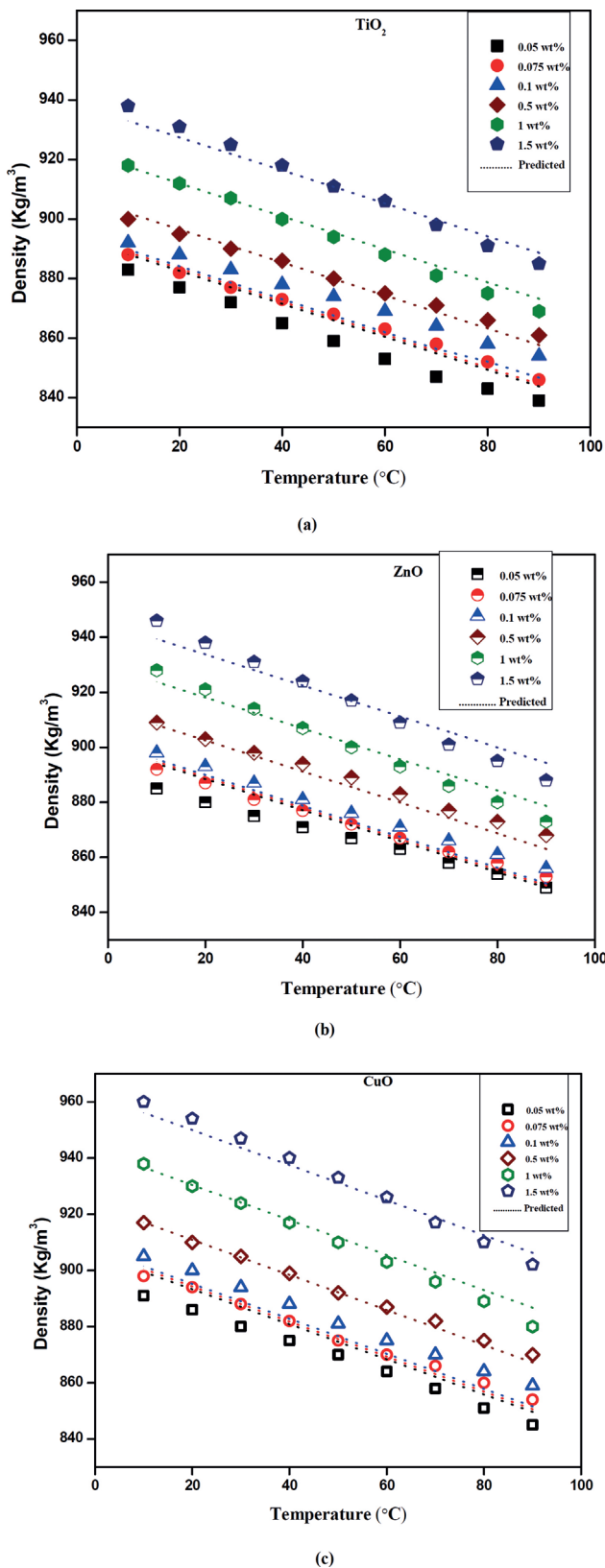


**Figure 14.** Density of (a) TiO<sub>2</sub>/Therminol-55 (b) ZnO/Therminol-55 and (c) CuO/Therminol-55 nanofluids as a function of temperature with different particle concentration.

(0.05wt%-1.5wt%) are Figure 14a. It shows that the density of nanofluids tends to increase with particle concentration and reduces with increase in temperature. The maximum increase of 938 kg/m<sup>3</sup> in density of TiO<sub>2</sub>/Therminol-55 based nanofluid was found to be at the particle concentration of 1.5wt% and at 10°C. The density for ZnO/Therminol-55 nanofluid at varying particle concentrations with different temperatures illustrated in Figure 14b. It is witnessed that the value of density for ZnO/Therminol-55 nanofluid is higher compared to the base fluid for every particle concentration. The highest value of 946 kg/m<sup>3</sup> in density of ZnO/Therminol-55 nanofluid was observed at the concentration of 1.5wt% and at 10°C. The density of CuO/Therminol-55 nanofluid with different temperatures for the particle concentrations of 0.05wt%-1.5wt% are shown in Figure 14c. It can be seen that, with the addition of nanoparticles in base fluid, density of nanofluid intensifies and this amount decreases with increase in temperature. Maximum value of 960 kg/m<sup>3</sup> in density of CuO/Therminol-55 nanofluid was observed at concentration of 1.5wt% at 10°C temperature. This trend is in agreement with the results of Said and Saidur (66) and Elias et.al. (67).

At 1.5wt% concentration, density of TiO<sub>2</sub>/Therminol-55, ZnO/Therminol-55 and CuO/Therminol-55 nanofluids is found to be decreased by 5.65%, 5.33% and 6.04% respectively when the temperature is elevated from 10°C to 90°C. Similarly for base fluid, when the temperature is increased from 10°C to 90°C, density gets reduced by 6.14%. A typical common trend was observed among all the nanofluids. Density of nanofluids increased when the particle concentration increased from 0.05wt% to 1.5wt%. This is due to the higher density of solid nanoparticles added (68) in base fluids. The nanoparticles possess very high density as compared to the base fluid. Therefore, increasing the nanoparticle concentration may result in an elevation in the density of nanofluids. An abrupt increase in the density of nanofluids due to the addition of nanoparticles used in various thermal and heat transfer applications is not desirable and may deteriorate convective heat transfer characteristic (69).

As there is not sufficient literature available about the densities of therminol-55 based nanofluids, therefore to validate the measured data, the experimental results were compared with the equation available in literature. Experimental results of the density of nanofluids at 20°C and the densities predicted by the Pak and Cho model are shown in Figure 15.

Pak and Cho proposed the equation as:

$$\rho_{nf} = (1 - \varphi)\rho_f + \varphi\rho_p \quad (8)$$

Figure 15 shows the predicted results of Pak and Cho model of nanofluids and experimental data. As shown in the figure, the values of Pak and Cho model is lower as compared to experimental data. The above equation failed to predict the enhancement in density of nanofluids. Thus,

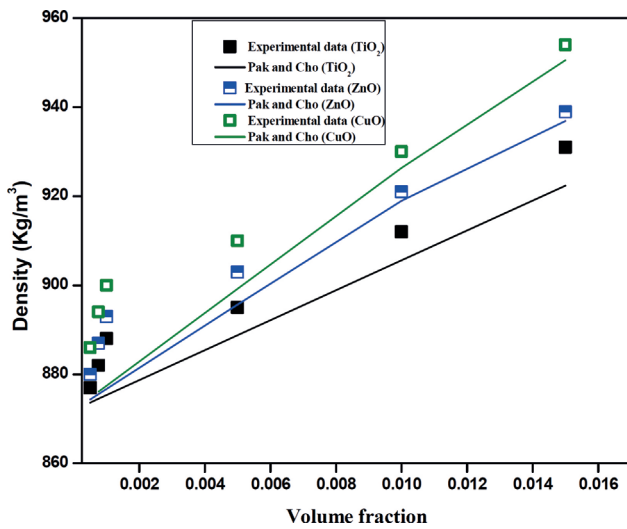


**Figure 15.** The comparative plots for the experimental density and theoretical model at 20°.

**Table 4.** Correlations for density of nanofluids with regression coefficient

Nanofluid	Correlation	Regression Coefficient
TiO <sub>2</sub> /Therminol-55	$\rho_{nf} = 892.133663 - 0.554444T + 30.931341\phi$	96.81%
ZnO/Therminol-55	$\rho_{nf} = 898.113685 - 0.563056T + 31.252748\phi$	97.05%
CuO/Therminol-55	$\rho_{nf} = 903.810886 - 0.623611T + 39.068464\phi$	97.91%

there was a need to develop a new multivariable correlation based on the corresponding experimental data for all the nanofluids as a function of particle concentration and temperature. The results were correlated with the equations and regression coefficients given in the Table 4.

## MEASUREMENT OF SURFACE TENSION OF NANOFLUIDS

### Effect of particle concentration surface tension

Figure 16 shows the variation in surface tension with respect to the concentration of nanoparticles added. The surface tension was measured at a temperature of 25°C with varying particle loading of 0.05 wt% to 1.5 wt%. It is evident that with the increase in particle concentration, decrease in surface tension is noted. The trends in surface tension were consistent with the findings of Ranjar et.al. (70) for  $\gamma$ -Al<sub>2</sub>O<sub>3</sub> and MgO nanoparticles added in Tri Ethylene Glycol nanofluid and with the observation of Pantzail et al. (71) for

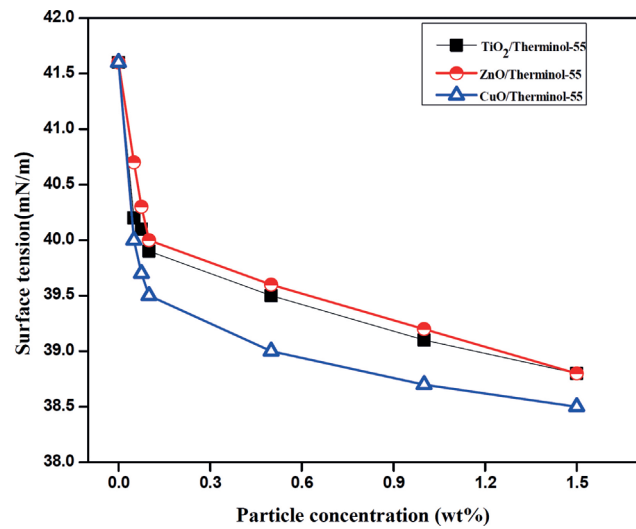


**Figure 16.** Surface tension of nanofluids with respect to the change in particle concentration.

CuO/water nanofluids observed that the surface tension steadily decreased up to 2% particle concentration.

The surface tension of nanofluids decreased with increasing particle concentration and can be attributed to the combined effect of surfactant and nanoparticles added in the base fluid. Higher the content of surfactant and nanoparticles added greater will be the reduction in surface tension of nanofluids. The decline in surface tension of nanofluids is due to the possible addition of surfactant for the stabilization of the suspension. These surfactants get absorbed on the surface of nanoparticles, and induce an electrostatic repulsive force between the particles, which appreciably decreases the surface tension of nanofluids.

## CONCLUSIONS

This study determined the thermo-physical properties such as: thermal conductivity, density and surface tension of TiO<sub>2</sub>/Therminol-55, ZnO/Therminol-55 and CuO/Therminol-55 nanofluids as a function of particle concentration and temperature. Stability of nanofluids was achieved by using Oleic acid as dispersant. For structural evaluation of nanoparticles various characterization techniques were used. Based on the current measurements, the following conclusions are summarized: -

- Experimental results for thermal conductivity show that both nanoparticle concentration and temperature have pronounced effect on thermal conductivity enhancement. The maximum improvement in thermal conductivity for TiO<sub>2</sub>/Therminol-55, ZnO/Therminol-55 and CuO/Therminol-55 nanofluids are reported to be 17.62%, 21.55% and 24.32% for the particle concentration of 1.5 wt%.

- ii. The theoretical explanations related to clustering of nanoparticles, molecular collisions and Brownian motion together affirm a considerable contribution on the enhancement of nanofluid thermal conductivity which has been demonstrated in current study.
- iii. The density of nanofluids increased significantly with increase in particle concentration and decrease dramatically with increase in temperature. Increase in density is due to the higher density of solid nanoparticles added in base fluid.
- iv. Comparison of the present study with the theoretical models for thermal conductivity and density, shows a significant deviation from the observed results for all the three different mono samples. Thus, new correlations were developed for each nanofluid including the particle concentration and temperature based on the experimental data.
- v. Experimental results demonstrate that the surface tension of nanofluids decrease with increase in nanoparticle loading. The presence of surfactant and absorption of nanoparticles at interface were identified as mechanisms for reduced surface tension of nanofluids.
- vi. For further heat transfer characteristics, investigation of other thermo-physical properties such as viscosity and specific heat and development of new correlations can be a future part of this work.

## NOMENCLATURE

EG	Ethylene Glycol
HTF	Heat Transfer Fluid
TiO <sub>2</sub>	Titanium oxide
ZnO	Zinc oxide
CuO	Copper oxide
MWCNT	Multi wall carbon nanotube
DWCNT	Double walled carbon nanotube
JCPDS	Joint committee on powder diffraction standards
Al <sub>2</sub> O <sub>3</sub>	Aluminum oxide
MgO	Magnesium oxide
CNT	Carbon nanotube
Bi <sub>2</sub> O <sub>3</sub>	Bismuth oxide
Cu	Copper
XRD	X-ray diffraction
FWHM	Full width half maximum
SEM	Scanning electron microscope
TEM	Transmission electron microscope
FTIR	Fourier transform infra-red
TGA	Thermogravimetric analysis
DTGA	Derivative thermogravimetric analysis
DSC	Differential scanning calorimetry
PV	Photovoltaic
W	Weight (gram)
k	Thermal conductivity (W/mK)

T	Temperature (°C)
nm	Nanometer
kV	Kilovolt
kHz	Kilo hertz

## Greek Symbols

φ	Volume fraction
λ	Wavelength (Angstrom)
ρ	Density (kg/m <sup>3</sup> )

## Subscripts

np	Nanoparticle
nf	Nanofluid
bf	Basefluid

## AUTHORSHIP CONTRIBUTIONS

Authors equally contributed to this work.

## DATA AVAILABILITY STATEMENT

The authors confirm that the data that supports the findings of this study are available within the article. Raw data that support the finding of this study are available from the corresponding author, upon reasonable request.

## CONFLICT OF INTEREST

The author declared no potential conflicts of interest with respect to the research, authorship, and/or publication of this article.

## ETHICS

There are no ethical issues with the publication of this manuscript.

## REFERENCES

- [1] Al-Amri F, Hassanain NAM, Al-Amri NF, Alzohbi G. An experimental study of solar panel performance using heat pipe and thermoelectric generator. *Int J Renew Energy Res* 2019;9:1418–1427. [\[CrossRef\]](#)
- [2] Roslan MEBM, Hassim I. Solar PV system with pulsating heat pipe cooling. *Indones J Electr Eng Comput Sci* 2019;14:311–318. [\[CrossRef\]](#)
- [3] Eltaweel M, Abdel-Rehim AA, Attia AAA. Energetic and exergetic analysis of a heat pipe evacuated tube solar collector using MWCNT/water nanofluid. *Case Stud Therm Eng* 2020;22:100743. [\[CrossRef\]](#)
- [4] Kholi FK, Mucci A, Kallath H, Ha MY, Chetwynd-Chatwin J, Min JK. Experimental investigation of the effects of inclinations and wicks on the thermal behavior of heat pipes for improved thermal

- applications. *Case Stud Therm Eng* 2021;26:100997. [\[CrossRef\]](#)
- [5] Ozsoy A, Corumlu V. Thermal performance of a thermosyphon heat pipe evacuated tube solar collector using silver-water nanofluid for commercial applications. *Renew Energy* 2018;122:26–34. [\[CrossRef\]](#)
- [6] Teng TP, Hsu HG, Mo HE, Chen CC. Thermal efficiency of heat pipe with alumina nanofluid. *J Alloys Compd* 2010;504(Suppl 1):S380–S384. [\[CrossRef\]](#)
- [7] Naphon P, Assadamongkol P, Borirak T. Experimental investigation of titanium nanofluids on the heat pipe thermal efficiency. *Int Commun Heat Mass Transf* 2008;35:1316–1319. [\[CrossRef\]](#)
- [8] Farahbod F. Investigation of thermal performance of a new drill equipped with heat pipe and nanofluid. *Case Stud Therm Eng* 2021;27:101316. [\[CrossRef\]](#)
- [9] Mbulu H, Laoonual Y, Wongwises S. Experimental study on the thermal performance of a battery thermal management system using heat pipes. *Case Stud Therm Eng* 2021;26:101029. [\[CrossRef\]](#)
- [10] Premkumar A, Senthilkumar S, Suryakumar B, Manikandan M. Research on impact of nanofluids in heat pipes. *Int J Eng Adv Technol* 2019;8(6 Suppl 3):1162–1165. [\[CrossRef\]](#)
- [11] Sonawane PM, Shende MD, Baisane VP. *IJEAS0301020.pdf*. 2016:31–35.
- [12] Kaggwa A, Carson JK. Developments and future insights of using nanofluids for heat transfer enhancements in thermal systems: a review of recent literature. *Int Nano Lett* 2019;9:277–288. [\[CrossRef\]](#)
- [13] Yashawantha KM, Vinod AV. Experimental investigation on thermal conductivity and stability of water-graphite nanofluid. *J Therm Eng* 2021;7:1743–1751. [\[CrossRef\]](#)
- [14] Estellé P, Halefadi S, Maré T. Thermal conductivity of CNT water based nanofluids: Experimental trends and models overview. *J Therm Eng* 2015;1:381–390. [\[CrossRef\]](#)
- [15] Choi SUS. Enhancing thermal conductivity of fluids with nanoparticles. *Am Soc Mech Eng Fluids Eng Div FED* 1995;231:99–105.
- [16] Muraleedharan M, Singh H, Suresh S, Udayakumar M. Directly absorbing Therminol-Al<sub>2</sub>O<sub>3</sub> nano heat transfer fluid for linear solar concentrating collectors. *Sol Energy* 2016;137:134–142. [\[CrossRef\]](#)
- [17] Anish M, Jayaprabakar J, Jayaprakash V, Prabhu A, Bhuvanesh Ram V, Austin Jijo M. Measurement dependent temperature of thermal conductivity and viscosity by using Al<sub>2</sub>O<sub>3</sub>-Therminol 55 based nanofluid. *Mater Today Proceed* 2020;21:332–334. [\[CrossRef\]](#)
- [18] Saidur R, Leong KY, Mohammed HA. A review on applications and challenges of nanofluids. *Renew Sustain Energy Rev* 2011;15:1646–1668. [\[CrossRef\]](#)
- [19] Dong F, Wan J, Feng Y, Wang Z, Ni J. Experimental study on thermophysical properties of propylene glycol-based graphene nanofluids. *Int J Thermophys* 2021;42:1–18. [\[CrossRef\]](#)
- [20] Estellé P, Cabaleiro D, Żyła G, Lugo L, Murshed SMS. Current trends in surface tension and wetting behavior of nanofluids. *Renew Sustain Energy Rev* 2018;94:931–944. [\[CrossRef\]](#)
- [21] Vajjha RS, Das DK, Mahagaonkar BM. Density measurement of different nanofluids and their comparison with theory. *Pet Sci Technol* 2009;27:612–624. [\[CrossRef\]](#)
- [22] Elias MM, Mahbulul IM, Saidur R, Sohel MR, Shahrul IM, Khaleduzzaman SS, et al. Experimental investigation on the thermo-physical properties of Al<sub>2</sub>O<sub>3</sub> nanoparticles suspended in car radiator coolant. *Int Commun Heat Mass Transf* 2014;54:48–53. [\[CrossRef\]](#)
- [23] Ravi Babu S, Sambasivarao G. Thermo-physical properties of water +ethylene glycol based alumina nanofluids. *J Mech Eng Res Dev* 2018;41:168–176.
- [24] Nabati Shoghl S, Jamali J, Keshavarz Moraveji M. Electrical conductivity, viscosity, and density of different nanofluids: An experimental study. *Exp Therm Fluid Sci* 2016;74:339–346. [\[CrossRef\]](#)
- [25] Xie H, Zhao Z, Zhao J, Gao H. Measurement of thermal conductivity, viscosity and density of ionic liquid [EMIM][DEP]-based nanofluids. *Chinese J Chem Eng* 2016;24:331–338. [\[CrossRef\]](#)
- [26] Jacquemin J, Husson P, Padua AAH, Majer V. Density and viscosity of several pure and water-saturated ionic liquids. *Green Chem* 2006;8:172–180. [\[CrossRef\]](#)
- [27] Selvakumar RD, Wu J. A comprehensive model for effective density of nanofluids based on particle clustering and interfacial layer formation. *J Mol Liq* 2019;292:111415. [\[CrossRef\]](#)
- [28] Ilyas SU, Pendyala R, Narahari M. Stability and thermal analysis of MWCNT-thermal oil-based nanofluids. *Colloids Surf A Physicochem Eng Asp* 2017;527:11–22. [\[CrossRef\]](#)
- [29] Wanic M, Cabaleiro D, Hamze S, Fal J, Estellé P, Żyła G. Surface tension of ethylene glycol-based nanofluids containing various types of nitrides: An experimental study. *J Therm Anal Calorim* 2020;139:799–806. [\[CrossRef\]](#)
- [30] Harikrishnan AR, Dhar P, Agnihotri PK, Gedupudi S, Das SK. Effects of interplay of nanoparticles, surfactants and base fluid on the surface tension of nanocolloids. *Eur Phys J E Soft Matter* 2017;40:51. [\[CrossRef\]](#)
- [31] Gulzar O, Qayoum A, Gupta R. Experimental study on thermal conductivity of mono and hybrid Al<sub>2</sub>O<sub>3</sub>-TiO<sub>2</sub> nanofluids for concentrating solar collectors. *Int J Energy Res* 2020;44:6956–6970. [\[CrossRef\]](#)

- [32] Gulzar O, Qayoum A, Gupta R. Photo-thermal characteristics of hybrid nanofluids based on Therminol-55 oil for concentrating solar collectors. *Appl Nanosci* 2019;9:1133–1143. [\[CrossRef\]](#)
- [33] Gulzar O, Qayoum A, Gupta R. Experimental study on stability and rheological behaviour of hybrid Al<sub>2</sub>O<sub>3</sub>-TiO<sub>2</sub> Therminol-55 nanofluids for concentrating solar collectors. *Powder Technol* 2019;352:436–444. [\[CrossRef\]](#)
- [34] Pak BC, Cho YI. Hydrodynamic and heat transfer study of dispersed fluids with submicron metallic oxide particles. *Exp Heat Transfer* 1998;11:151–170. [\[CrossRef\]](#)
- [35] Manikandan S, Rajan KS. MgO-Therminol 55 nanofluids for efficient energy management: Analysis of transient heat transfer performance. *Energy* 2015;88:384–394. [\[CrossRef\]](#)
- [36] Toghraie D, Chaharsoghi VA, Afrand M. Measurement of thermal conductivity of ZnO-TiO<sub>2</sub>/EG hybrid nanofluid. *J Therm Anal Calorim* 2016;125:73–81. [\[CrossRef\]](#)
- [37] Naresh Y, Dhivya A, Suganthi KS, Rajan KS. High-temperature thermo-physical properties of novel CuO-therminol<sup>®</sup>55 nanofluids. *Nanosci Nanotechnol Lett* 2012;4:1209–1213. [\[CrossRef\]](#)
- [38] Ali N, Teixeira JA, Addali A. A review on nanofluids: fabrication, stability, and thermophysical properties. *J Nanomater* 2018;2018:4257136. [\[CrossRef\]](#)
- [39] Khan M, Naqvi AH, Ahmad M. Comparative study of the cytotoxic and genotoxic potentials of zinc oxide and titanium dioxide nanoparticles. *Toxicol Rep* 2015;2:765–774. [\[CrossRef\]](#)
- [40] Ba-Abbad MM, Kadhum AAH, Mohamad AB, Takriff MS, Sopian K. Synthesis and catalytic activity of TiO<sub>2</sub> nanoparticles for photochemical oxidation of concentrated chlorophenols under direct solar radiation. *Int J Electrochem Sci* 2012;7:4498–4511.
- [41] Hema M, Arasi Ay, Tamilselvi P, Anbarasan R. Titania nanoparticles synthesized by sol-gel technique. *Chem Sci Trans* 2012;2:246–252. [\[CrossRef\]](#)
- [42] Tettey CO, Shin HM. Evaluation of the antioxidant and cytotoxic activities of zinc oxide nanoparticles synthesized using scutellaria baicalensis root. *Sci African* 2019;6:e00168. [\[CrossRef\]](#)
- [43] Safawo T, Sandeep BV, Pola S, Tadesse A. Synthesis and characterization of Zinc oxide nanoparticles using tuber extract of anchote (*Coccinia abyssinica* (Lam.) Cong.) for antimicrobial and antioxidant activity assessment. *OpenNano* 2018;3:43–52. [\[CrossRef\]](#)
- [44] Kumar H, Rani R. Structural and optical characterization of ZnO nanoparticles synthesized by microemulsion route. *Int Lett Chem Phys Astron* 2013;19:26–36. [\[CrossRef\]](#)
- [45] Nejati K, Rezvani Z, Pakizevand R. Synthesis of ZnO Nanoparticles and Investigation of the Ionic Template Effect on Their Size and Shape. *Int Nano Lett* 2011;1:81–88.
- [46] Mohamed EA. Green synthesis of copper & copper oxide nanoparticles using the extract of seedless dates. *Heliyon* 2020;6:e03202. [\[CrossRef\]](#)
- [47] Raul PK, Senapati S, Sahoo AK, Umlong IM, Devi RR, Thakur AJ, et al. CuO nanorods: A potential and efficient adsorbent in water purification. *RSC Adv* 2014;4:40106–40112. [\[CrossRef\]](#)
- [48] Tsai W-B, Kao J-Y, Wu T-M, Cheng W-T. Dispersion of Titanium Oxide Nanoparticles in Aqueous Solution with Anionic Stabilizer via Ultrasonic Wave. *J Nanoparticles* 2016;2016:1252685. [\[CrossRef\]](#)
- [49] Mehrali M, Sadeghinezhad E, Latibari ST, Kazi SN, Mehrali M, Zubir MNBM, et al. Investigation of thermal conductivity and rheological properties of nanofluids containing graphene nanoplatelets. *Nanoscale Res Lett* 2014;9:1–12. [\[CrossRef\]](#)
- [50] Sadoughi K, Hosseini M, Shakeri F, Azimi M. Analytical simulation of MHD nanofluid flow over the horizontal plate. *Front Aerosp Eng* 2013;2:318–326. [\[CrossRef\]](#)
- [51] Turgut A, Tavman I, Chirtoc M, Schuchmann HP, Sauter C, Tavman S. Thermal conductivity and viscosity measurements of water-based TiO<sub>2</sub> nanofluids. *Int J Thermophys* 2009;30:1213–1226. [\[CrossRef\]](#)
- [52] Mukherjee S, Panda SR, Mishra PC, Chaudhuri P. Enhancing Thermophysical Characteristics and Heat Transfer Potential of TiO<sub>2</sub>/Water Nanofluid. *Int J Thermophys* 2020;41:126. [\[CrossRef\]](#)
- [53] Afrand M, Toghraie D, Sina N. Experimental study on thermal conductivity of water-based Fe<sub>3</sub>O<sub>4</sub> nanofluid: Development of a new correlation and modeled by artificial neural network. *Int Commun Heat Mass Transf* 2016;75:222–229. [\[CrossRef\]](#)
- [54] Abdul Hamid K, Azmi WH, Mamat R, Usri NA. Thermal conductivity enhancement of TiO<sub>2</sub> nanofluid in water and ethylene glycol (EG) mixture. *Indian J Pure Appl Phys* 2016;54:620–626.
- [55] Sezer N, Atieh MA, Koç M. A comprehensive review on synthesis, stability, thermophysical properties, and characterization of nanofluids. *Powder Technol* 2019;344:706–742. [\[CrossRef\]](#)
- [56] Moosavi M, Goharshadi EK, Youssefi A. Fabrication, characterization, and measurement of some physicochemical properties of ZnO nanofluids. *Int J Heat Fluid Flow* 2010;31:606–613. [\[CrossRef\]](#)
- [57] Rostami S, Nadooshan AA, Raisi A. An experimental study on the thermal conductivity of new anti-freeze containing copper oxide and graphene oxide nano-additives. *Powder Technol* 2019;345:186–193. [\[CrossRef\]](#)

- [58] Ahmadi Nadooshan A. An experimental correlation approach for predicting thermal conductivity of water-EG based nanofluids of zinc oxide. *Phys E Low-Dimensional Syst Nanostructures* 2017;87:134–138. [\[CrossRef\]](#)
- [59] Esfahani MA, Toghraie D. Experimental investigation for developing a new model for the thermal conductivity of Silica/Water-Ethylene glycol (40%–60%) nanofluid at different temperatures and solid volume fractions. *J Mol Liq* 2017;232:407–417. [\[CrossRef\]](#)
- [60] Xie H, Wang J, Xi T, Liu Y, Ai F, Wu Q. Thermal conductivity enhancement of suspensions containing nanosized alumina particles. *J Appl Phys* 2002;91:4568–4572. [\[CrossRef\]](#)
- [61] Suganthi KS, Radhakrishnan AK, Anusha N, Rajan KS. Influence of nanoparticle concentration on thermo-physical properties of CuO-propylene glycol nanofluids. *J Nanosci Nanotechnol* 2014;14:4168–4173. [\[CrossRef\]](#)
- [62] Said Z, Sajid MH, Alim MA, Saidur R, Rahim NA. Experimental investigation of the thermophysical properties of AL<sub>2</sub>O<sub>3</sub>-nanofluid and its effect on a flat plate solar collector. *Int Commun Heat Mass Transf* 2013;48:65. [\[CrossRef\]](#)
- [63] Clerk JM. *A Treatise on Electricity and Magnetism*. Vol. 9781108014. Cambridge: Cambridge University Press; 2010. [\[CrossRef\]](#)
- [64] Hamilton RL. Thermal conductivity of heterogeneous two-component systems. *Ind Eng Chem Fundam* 1962;1:187–191.
- [65] Van Trinh P, Anh NN, Thang BH, Quang LD, Hong NT, Hong NM, et al. Enhanced thermal conductivity of nanofluid-based ethylene glycol containing Cu nanoparticles decorated on a Gr-MWCNT hybrid material. *RSC Adv*. 2017;7:41–49. [\[CrossRef\]](#)
- [66] Said Z, Saidur R. Thermophysical Properties of Metal Oxides Nanofluids. In: Mohsen Sheikholeslami K, Ellahi R, Rashidi MM, Eds. *Nanofluid Heat Mass Transf Eng Probl*. Cham: Springer International Publishing; 2017. p. 13–24. [\[CrossRef\]](#)
- [67] Elias MM, Mahbulul IM, Saidur R, Sohel MR, Shahrul IM, Khaleduzzaman SS, et al. Experimental investigation on the thermo-physical properties of Al<sub>2</sub>O<sub>3</sub> nanoparticles suspended in car radiator coolant. *Int Commun Heat Mass Transf* 2014;54:48–53. [\[CrossRef\]](#)
- [68] Elsaid K, Abdelkareem MA, Maghrabie HM, Sayed ET, Wilberforce T, Baroutaji A, et al. Thermophysical properties of graphene-based nanofluids. *Int J Thermofluids* 2021;10:100075. [\[CrossRef\]](#)
- [69] Ilyas SU, Narahari M, Theng JTY, Pendyala R. Experimental evaluation of dispersion behavior, rheology and thermal analysis of functionalized zinc oxide-paraffin oil nanofluids. *J Mol Liq* 2019;294:111613. [\[CrossRef\]](#)
- [70] Ranjbar H, Khosravi-Nikou MR, Safiri A, Bovard S, Khazaei A. Experimental and theoretical investigation on Nano-fluid surface tension. *J Nat Gas Sci Eng* 2015;27:1806–1813. [\[CrossRef\]](#)
- [71] Pantzali MN, Kanaris AG, Antoniadis KD, Mouza AA, Paras SV. Effect of nanofluids on the performance of a miniature plate heat exchanger with modulated surface. *Int J Heat Fluid Flow* 2009;30:691–699. [\[CrossRef\]](#)